Metasurface holograms reaching 80% overall efficiency

Guoxing Zheng[1, 2*], Holger Mühlenbernd[3*], Mitchell Kenney[1*], Guixin Li[4†], Thomas Zentgraf[3‡] and Shuang Zhang[1§]

1. *School of Physics & Astronomy, University of Birmingham, Birmingham, B15 2TT, UK*
2. *School of Electronic Information, Wuhan University, Wuhan, 430072, China*
3. *Department of Physics, University of Paderborn, Warburger Straße 100, D-33098 Paderborn, Germany*
4. *Department of Physics, Hong Kong Baptist University, HongKong, China*

Abstract: Geometric phase metasurfaces (GEMS) consisting of nanorods with spatially varying orientations are capable of generating continuous phase profiles in the subwavelength scale and therefore facilitate new perspectives in designing complicated phase-only Computer Generated Holograms (CGHs). Previously demonstrated geometric metasurfaces, however, suffer from low efficiency at visible wavelengths. Here we report the design and realization of highly efficient geometric phase metasurfaces. A 16-level phase CGH design is realized using the metasurface, exhibiting high quality holographic images with very high fidelity and a broad bandwidth between 630 nm and 1050 nm. Importantly, the overall efficiency, defined as the ratio of light intensity forming the holographic image to that of the incident light, reaches 80%, greatly surpassing previously demonstrated metasurface based CGH. The GEMS based CGHs with their accurate phase modulation, high efficiency, and simple fabrication procedure compared to conventional multi-step phase holograms, are highly promising for various practical applications ranging from laser holographic projection to data storage and beam shaping.

In traditional phase-only computer generated hologram designs, the phase profile is controlled by etching different depths into a transparent substrate. Due to the ease of fabrication, two level binary CGHs have been widely employed. Such CGHs have a theoretical diffraction efficiency of only 40.5% and the issue of twin-image generation cannot be avoided. Multi-level phase CGHs can alleviate the problem of low efficiency and twin-image generation; however, fabricating such CGHs requires expensive and complicated grayscale lithography, variable-dose, or multi-step lithography[1]. Furthermore, the unavoidable etching error, resolution error and alignment error can dramatically degrade the performance of CGHs, such as low signal-to-noise ratio, poor uniformity and strong zero-order intensity. To obtain a higher efficiency and less manufacturing complexity, an effective medium approach has been proposed[1], where two-level depth subwavelength structures with variable cell dimension can function as an effective medium with geometry controlled effective refractive index, and consequently act as a multi-level CGH.

* These authors contributed equally to this work.
† gxli@hkbu.edu.hk
‡ thomas.zentgraf@uni-paderborn.de
§ s.zhang@bham.ac.uk

However, such a design involves extreme small feature sizes with high aspect ratios, limiting the observed efficiency of a three level CGH to less than 30%, which is significantly lower than the theoretical value of 48%.

In recent years, complete phase control with ultrathin plasmonic structures, so called metasurfaces[2,3,4,5,6,7,8,9,10,11,12,13] have been developed, which represent a new paradigm for the design of innovative optical elements. Metasurfaces have been recently applied to CGHs[14,15,16,17,18,19,20]. However, most of the demonstrated diffraction efficiency of the metamaterial based CGHs is far lower than that of traditional holography. Scheuer *et al.*[17] proposed patch-dipole nanoantenna reflectarrays where the phase profile is controlled by varying the geometrical size and position of each individual nanoantenna. The efficiency reaches 40% - 50% in the far-infrared range, the highest among various plasmonic or metasurface based CGHs, but only at par with the traditional two level CGHs. In addition, the patch-dipole reflectarray requires delicately controlled geometry to achieve a desired phase profile while maintaining a uniform amplitude, which would limit the number of phase levels for improving the CGH efficiency.

Among various types of metasurfaces, geometric metasurfaces (GEMS) that consist of an array of plasmonic nanorods with spatially varying orientations, have shown superior phase control due to the geometric nature of the phase. GEMS have been utilized to generate 3-D holography[18], diffractive gratings[21] and dual polarity lenses[5,13]. However, GEMS operating at visible and near infrared wavelengths have been limited so far by the low efficiency in conversion between the two circular polarization states. In this letter, we combine the concept of GEMS for the superior control of the phase profile[4] and the concept of reflectarrays for achieving high polarization conversion efficiency[22,23,24,25,26] to demonstrate a high quality GEMS hologram with ultrahigh efficiency. The GEMS hologram shows continuously controllable phase profiles with overall efficiency exceeding 80%. This high efficiency is comparable to most of the traditional multi-level depth-controlled CGHs but with much simpler fabrication, only involving a single lithography step. Moreover, the GEMS holograms show advantages such as continuous phase modulation, pure planar configuration, and broad spectral response. This novel geometric phase based CGH technology may replace traditional depth-controlled CGH in various applications, such as laser holographic projection, random spots generator for body motion, laser beam shaping, and optical information processing.

The operation of GEMS relies on the inversion of the absolute rotation direction of the electric field of the radiation (in transmission or reflection) compared to that of the incident circularly polarized one. This is equivalent of flipping the circular polarization in transmission or maintaining the same circular polarization in reflection. A geometric phase, or Pancharatnam-Berry phase, is acquired through the inversion of electric field rotation, leading to an antenna-orientation controlled phase which does not depend on the specific antenna design or wavelength, thus making its performance broadband, and highly robust against fabrication latitude and variation of material properties. To dramatically increase the conversion efficiency, we design a reflective metasurface consisting of three layers: a ground metal plane, a dielectric spacer layer and a top layer of antennas (Figure 1). It is well known that a half wave plate can

fully convert a circular polarized beam to the oppositely polarized one in transmission due to a phase delay of π between the fast and slow axis. Hence, for achieving high conversion between the two circular polarization states, it is desired that the phase difference between the reflection with polarization along the long axis (r_l) and short axis (r_s) of the nanorod antenna equals π. The simulated results in Figure 1d-e show that, with an optimized configuration, the phase difference between the reflection coefficients r_l and r_s approaches π within a wide wavelength range of 600-1000 nm. At the same time, the configuration maintains very large reflection amplitudes over 0.8 for both linear polarizations. Therefore, regardless the orientation of the antennas, it is expected that the circularly polarized incident light almost completely flips the absolute rotation direction of the electric field upon reflection, thus preserving its circular polarization state considering that the wave vector is reversed as well. This forms the basis of the high efficiency geometric metasurface. A detailed discussion and a simplified model for explaining the high efficiency and broadband responses of the nanorod metasurface can be found in the Supplementary Information.

The high efficiency of maintaining the same circular polarization state upon reflection is verified by numerical simulations for a uniform metasurface with all nanorod antennas aligned along the same direction, as shown in Figure 1f. The reflected wave in general consists of both circular polarization states: one is the same handedness as the incident circularly polarized light but with an additional phase delay 2ϕ, where ϕ is the orientation angle of the nanorod antenna, and the other one is the opposite handedness without the additional phase delay[4]. For the specific geometry configuration shown in Figure 1a upon normal light incidence, the numerical simulation shows that the reflectivity of light with the same circular polarization state is over 80% in a broad wavelength range between 550 nm and 1000 nm, covering nearly a full optical octave. This efficiency is surprisingly high considering the ohmic loss of metal at the visible and near infrared frequencies. On the other hand, the efficiency of the unwanted opposite polarization is extremely low, less than 3%, over a broad wavelength range.

For confirming the high efficiency of our numerical simulations we designed a geometric metasurface based CGH as shown in Figure 2. The CGH was designed for circularly polarized light at normal incidence. We used a design that the holographic image appears off-axis to avoid the overlapping between the holographic image and the zero-order spot. In the design, a complex digital image containing Einstein's portrait (copyright license from Free Stock Photos[27]) with pixel number of 550×300 and 256 greyscale levels was chosen as holographic target image (Figure 2b). The CGH is designed to create a wide image angle of 60°×30°. Because of the large angular range, the Rayleigh-Sommerfeld diffraction method is used to simulate the holographic image[28]. The hologram is pre-compensated to avoid the pattern distortion. To avoid the formation of laser speckles in the holographic image, the concept of Dammann gratings[29,30] is utilized for the hologram design. In our structure we used a 2×2 periodic array of the hologram pattern (Figure 2d), more details of the advantages of the 2x2 gratings over single hologram is given in of the Supplementary Information. To create an holographic image with a pixel array of $m \times n$ within the angular range of $\alpha_x \times \alpha_y$ in the far field, the period of CGH at x and y direction can be calculated by $d_x = m\lambda/[2\tan(\alpha_x/2)]$ and $d_y = n\lambda/[2\tan(\alpha_y/2)]$, respectively. The number of pixels of the CGH is determined by $M = d_x/\Delta p$ and $N = d_y/\Delta p$, where Δp is the pixel size of the CGH in both x and y

directions.

With the above structural parameters, a phase-only CGH with pixel size of 300nm×300nm and periods of 333.3μm×333.3μm was designed by the classical Gerchberg−Saxton algorithm[31]. The obtained phase distribution is shown in Figure 2c. In the CGH design, we take the conversion efficiency, signal-to-noise ratio and uniformity as merit functions for optimization. Since the phase delay is determined solely by the orientation of the nanorod antennas, 16 phase levels (Figure 1c) are used to obtain a high performance of the CGH. Simulation shows that in our optimized design with an ideal hologram neglecting optical losses, the window efficiency, which is defined as the ratio between the optical power projected into the image region and the input power, reaches 94%.

The metasurface CGH is fabricated on top of a Silicon substrate following the design described above. The metal ground plane and the spacer layer (MgF_2 film) are deposited using electron beam evaporation. Subsequently, the gold nanorod array is fabricated by using standard e-beam lithography (Figure 3a). For the imaging experiment, we used a red laser (He-Ne laser, wavelength of 632.8 nm) and a near infrared diode laser (780 nm). The circularly polarized laser source is incident onto the metasurface hologram, and the reflected holographic image is projected onto a white screen 300 mm away from the surface of the hologram. We captured the red and near infrared holographic image by using commercial digital cameras (Nikon D3200 and ELOP-Contour CMOS IR Digital Camera). The simulated and measured images, including both the zoomed-in views of the face and letter 'M', show good agreement with each other. This demonstrates the extremely high fidelity of the metasurface hologram.

For determine the conversion efficiency, the linear polarization state of light from a super continuum light source (Fianium supercontinuum) is converted to circular polarization by using a linear polarizer and a quarter waveplate. The reflected holographic image is collected by two condenser lenses with high numerical aperture and the hologram image was measured in the range from 600 nm to 1100 nm in steps of 25 nm. The optical efficiency (holographic window efficiency) is finally determined by subtracting the 0^{th}-order beam signal from the image intensity (Figure 3b). We find a relatively broad spectral range from 630 nm to 1050 nm with high window efficiency larger than 50% that reaches its maximum of 80% at a wavelength of 825 nm. At the same time the unwanted 0^{th}-order efficiency is only around 2.4%. More importantly, we do not observe the twin image effect that traditional binary holograms usually suffer from. To the best of our knowledge, this is the best holography result to date for all reported metamaterials based holograms in terms of both the image quality, operational bandwidth and conversion efficiency.

Theoretically the metasurface hologram has an even broader spectral response (Figure 1f) when compared to the measured efficiency. The lower bandwidth likely arises from the fact that the calculated conversion efficiency is obtained on a metasurface under normal incidence. Whereas in the experiment the holographic image from the metasurface hologram is projected into a broad angular range. We expected that this broad angle scattering induces the narrower bandwidth and lower peak reflection than the calculated results shown in Figure 1f. In addition, a weak near-field coupling effect among neighboring nanorod antennas introduces a small phase

deviation compared to the design. A detailed discussion of the simulated scattering characteristic of the nanorods and the near-field coupling can be found in the Supplementary Information.

In summary, we have presented a reflective phase-only hologram based on geometric metasurfaces with high efficiency and broadband spectral response. Experiments on such holograms verified our design and demonstrated that the maximum efficiency exceeds 80% with extremely low 0^{th}-order efficiency. With its simple and robust phase control, good tolerance to wavelength variations and fabrication errors, this novel geometric phase based CGH is expected to challenge the traditional depth-controlled CGH and find numerous applications in fields like laser holographic keyboard, random spots generator for body motion, optical anti-counterfeiting, and laser beam shaping. On the other hand, the GEMS hologram demonstrated here, with an ultrathin and uniform thickness, is compatible with the scalar diffraction theory even for subwavelength pixel sizes simplifying the design of such holograms[32,33]. Our GEMS hologram can be readily extended from phase-only to amplitude-controlled holograms by changing the size of nanorods. Since we are utilizing a phase effect due to the polarization state change, as the only restriction the polarization state of the light cannot be controlled by our technique. While the incident light has to be circularly polarized, circularly polarized light can be easily obtained and occurs also naturally in nature. There might be even applications where the circular polarization states are desired and therefore the preferred state. By utilizing a different fabrication method for the hologram like nano-imprinting[34], such nanorod metasurfaces could be potentially fabricated on larger scale with much lower costs, making them promising candidates for mass fabricated holograms in the future.

Acknowledgement

The research is partly supported by EPSRC. We thank Dr. Lingxiao Zhu and Dr. Wei He for fruitful discussions. H. M. and T. Z. acknowledge the financial support by the DFG Research Training Group GRK1464. S. Z. and T. Z. acknowledge the European Commission under the Marie Curie Career Integration Program.

Methods:

1. Simulation of the conversion efficiency. The nanorod cell was designed and simulated by CST microwave studio software[35]. In the simulation, a linearly polarized plane wave is normally incident onto a single nanorod with periodic boundary conditions. The spectra of reflection coefficients r_{xx}, r_{xy}, r_{yy}, r_{yx} are obtained from the simulation. From the reflection of linear polarized light we can retrieve the reflection coefficients for circularly polarized light as $r_{rr}=[r_{xx}+r_{yy}-(r_{xy}-r_{yx})\cdot i]/2$ and $r_{lr}=[r_{xx}-r_{yy}-(r_{yx}+r_{xy})\cdot i]/2$. The performance of the nanorods is optimized by sweeping the geometric parameters of the nanorod including the cell size, spacer and gold thickness.

2. Fabrication and experimental setup. The samples are fabricated on a gold and MgF_2-coated Silicon substrate with standard electron-beam lithography, subsequent deposition of 30 nm gold and lift-off processes. Figure 4 shows a schematic of the optical efficiency measurement setup. The polarization state of the laser source is converted to circularly polarization by passing through a linear polarizer and a quarter waveplate. A lens with focal length of 300 mm was used to focus the incident beam onto the hologram. Color filters are used to remove the unwanted

light generated by the fiber laser. In addition, an iris is used to block the scattered beam from multi-reflections between the optical interfaces. Two identical condenser lenses with high numerical aperture (N.A.=0.6) are used to collect and focus the diffracted light for the measurement by using a power meter in the wavelength range: 400 nm-1100 nm. The intensity of the light is measured at two points in the beam path, Point 1 and Point 2, as shown in Figure 4. The window efficiency η_W can be evaluated by:

$$\eta_W = \frac{P_2 - P_Z}{P_1} \cdot \frac{1}{T_c}, \qquad (1)$$

where P_z is optical power of zero-order beam, P_1 and P_2 are optical power measured at point 1 and 2, separately. T_c is the transmission efficiency of the two condenser lenses, which is obtained by ray tracing simulations and experimental measurement. For our off-axis hologram design, the zero-order beam is separated from the signal beam and can be captured and measured separately. More details about the experiment can be found in the Supplementary Information.

References:

[1]Freese, W., Kämpfe, T., Kley, E. B., & Tünnermann, A. Design of binary subwavelength multiphase level computer generated holograms. *Optics Lett.* 35(5), 676-678(2010).
[2]Yu, N. et al. Light propagation with phase discontinuities: generalized laws of reflection and refraction. *Science* 334, 333-337 (2012).
[3]Ni, X., Emani, N. K., Kildishev, A. V., Boltasseva, A. & Shalaev, V. M. Broadband light bending with plasmonic nano antennas. *Science* 335, 427 (2012).
[4]Huang, L. et al. Dispersionless phase discontinuities for controlling light Propagation. *Nano Lett*. 12, 5750-5755 (2012).
[5]Chen, X. et al. Dual-polarity plasmonic metalens for visible light. *Nature Comm*. 3, 1198 (2012).
[6]Sun, S. et al. Gradient-index meta-surfaces as a bridge linking propagating waves and surface waves. *Nature Mater*. 11, 426-431 (2012).
[7]Aieta, F. et al. Aberration-free ultrathin flat lenses and axicons at telecom wavelengths based on plasmonic metasurfaces. *Nano Lett*. 12, 4932-4936 (2012).
[8]Ni, X., Ishii, S., Kildishev, A. V. & Shalaev, V. M. Ultra-thin, planar, Babinet-inverted plasmonic metalenses. *Light Sci. & Appl*. 2, e72 (2013).
[9]Yin, X., Ye, Z., Rho, J., Wang, Y. & Zhang, X. Photonic spin hall effect at metasurfaces. *Science* 339, 1405-1407 (2013).
[10]Lin, J. et al. Polarization-controlled tunable directional coupling of surface plasmon polaritons. *Science* 340, 331-334 (2013).
[11]Shitrit, N. et al. Spin-optical metamaterial route to spin-controlled photonics. *Science* 340, 724-726 (2013).
[12]Huang, L. et al. Helicity dependent directional surface plasmon polariton excitation using a metasurface with interfacial phase discontinuity. *Light Sci. & Appl*. 2, e70 (2013).
[13]Chen, X.et al. Reversible Three-Dimensional Focusing of Visible Light with Ultrathin Plasmonic Flat Lens. Adv. Opt. Mater. 1(7), 517-521 (2013).
[14]Larouche, S., Tsai, Y. J., Tyler, T., Jokerst, N. M., & Smith, D. R. Infrared metamaterial phase holograms. *Nature Mater.* 11(5), 450-454 (2012).
[15]Walther, B., Helgert, C., Rockstuhl, C., & Pertsch, T. Diffractive optical elements based on plasmonic metamaterials. *Appl. Phys. Lett.* 98(19), 191101 (2011).
[16]Chen, W. T. et al. High-efficiency broadband meta-hologram with polarization-controlled dual images. *Nano Lett.* 14(1), 225-230 (2013).
[17]Yifat, Y., Eitan, M., Iluz, Z., Hanein, Y., Boag, A., & Scheuer, J. Highly Efficient and Broadband Wide-Angle Holography Using Patch-Dipole Nanoantenna Reflectarrays. *Nano Lett.* 14(5), 2485-2490 (2014).
[18]Huang, L.et al. Three-dimensional optical holography using a plasmonic metasurface. *Nature Commun.* 4 (2013).
[19]Ni, X., Kildishev, A. V., & Shalaev, V. M. Metasurface holograms for visible light. *Nature Commun*. 4 (2013).
[20]Lin, J., Genevet, P., Kats, M.A., Antoniou, N., & Capasso, F. Nanostructured holograms for broadband manipulation of vector beams. *Nano Lett.* 13(9), 4269-4274 (2013).
[21]Liu, L.et al. Broadband Metasurfaces with Simultaneous Control of Phase and Amplitude. *Adv. Mater.* 26(29), 5013-5036 (2014).
[22]Hao, J. et al. Manipulating Electromagnetic Wave Polarizations by Anisotropic Metamaterials, *Phys. Rev. Lett.* 99, 063908 (2007).
[23]Hao, J., Ren, Q., An, Z., Huang, X., Chen, Z., Qiu, M., & Zhou, L. Optical metamaterial for polarization control. *Phys. Rev. A* 80(2), 023807 (2009).
[24]Pors, A., Nielsen, M. G., & Bozhevolnyi, S. I. Broadband plasmonic half-wave plates in reflection. *Optics Lett.* 38(4), 513-515 (2013).
[25]Sun, S. et al. High-Efficiency Broadband Anomalous Reflection by Gradient Meta-Surfaces. *Nano Lett.* 12(12), 6223-6229 (2012).
[26]Grady, N. K. et al. Terahertz Metamaterials for Linear Polarization Conversion and Anomalous Refraction, *Science* 340, 1304 (2013).

[27]http://publicdomainpictures.net/view-image.php?image=8612
[28]Shen, F., & Wang, A. Fast-Fourier-transform based numerical integration method for the Rayleigh-Sommerfeld diffraction formula. *Appl. Opt*. 45(6), 1102-1110 (2006).
[29]Dammann, H., & Görtler, K. High-efficiency in-line multiple imaging by means of multiple phase holograms. *Opt. Comm.* 3(5), 312-315, (1971).
[30]Feldman, M. R., & Guest, C. C. Iterative encoding of high-efficiency holograms for generation of spot arrays. *Opt. Lett.* 14(10), 479-481 (1989).
[31]Gerchberg, R. W. & Saxton, W. O. A practical algorithm for the determination of phase from image and diffraction plane pictures. *Optik* 35, 237 (1972).
[32]Magnusson, R & Gaylord, T. K. Diffraction efficiencies of thin phase gratings with arbitrary grating shape, *J. Opt. Soc. Am.* 68 (1978).
[33]Hasman, E., Davidson, N., & Friesem, A. A. Efficient multilevel phase holograms for CO_2 lasers, *Opt. Lett.* 16, 423 (1991).
[34]Guo, L. J. Nanoimprint lithography: methods and material requirements. *Adv. Mater.* 19(4), 495-513 (2007).
[35]CST MWS version 2013; www.CST.com (accessed July 2013).

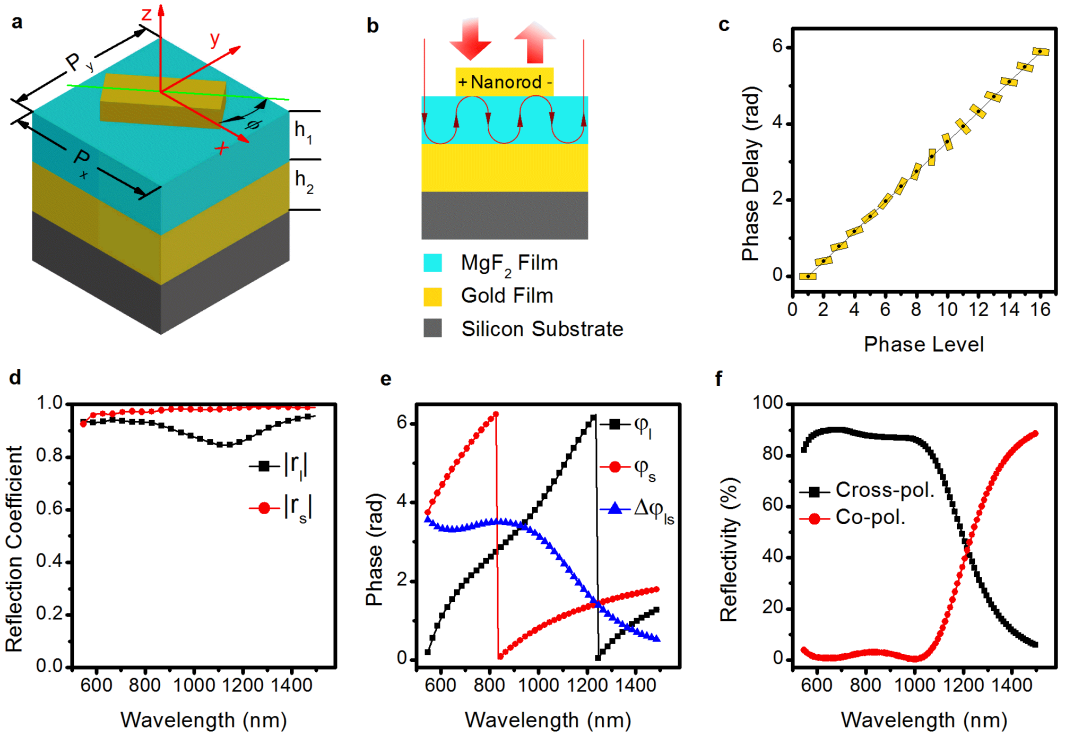

Figure 1 | Illustration of the unit-cell structure and its polarization conversion efficiency by numerical simulations. a, One pixel cell structure of the nanorod based hologram. The nanorod can rotate in the x-y plane with an orientation angle ϕ to create different phase delay. The pixels are arranged with periods P_x=300 nm and P_y=300 nm. The nanorods have a length of L=200 nm, a width of W=80 nm and a height of H=30 nm. The MgF_2 and gold film have thicknesses of h_1=90 nm and h_2=130 nm, respectively. **b**, Cross section of the pixel cell. The MgF_2 film acts as a Fabry-Pérot cavity, which can let the returned beam keep exciting the nanorod and generate the output beam with phase-delay. The gold film acts as the mirror to reflect the incident light. **c**, Phase delay for the different phase levels. On each knot, the orientation of nanorod has been annotated. **d and e**, Simulated amplitude and phase of the reflection coefficients r_l and r_s, where l and s denote the long and short axis directions of the nanorods, respectively. **f**, Simulated cross-polarization and co-polarization reflectivity upon normal light incidence.

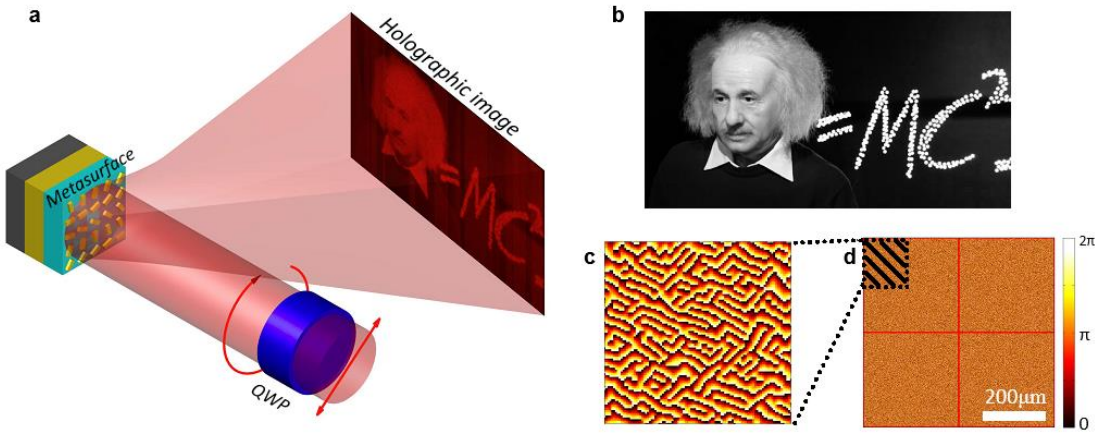

Figure 2 | Working principle and phase distribution of the periodic hologram. a, Illustration of the reflective nanorod-based CGH under a circularly polarized incident beam. **b**, Target image with 256 greyscale levels and a size of 550×300 pixels used for the generation of the hologram. **c and d**, To generate the target holographic image in the far field, the designed 16-level phase distribution with 2×2 periods is illustrated. An enlarged phase distribution with 100×100 pixels at up-left corner is shown separately.

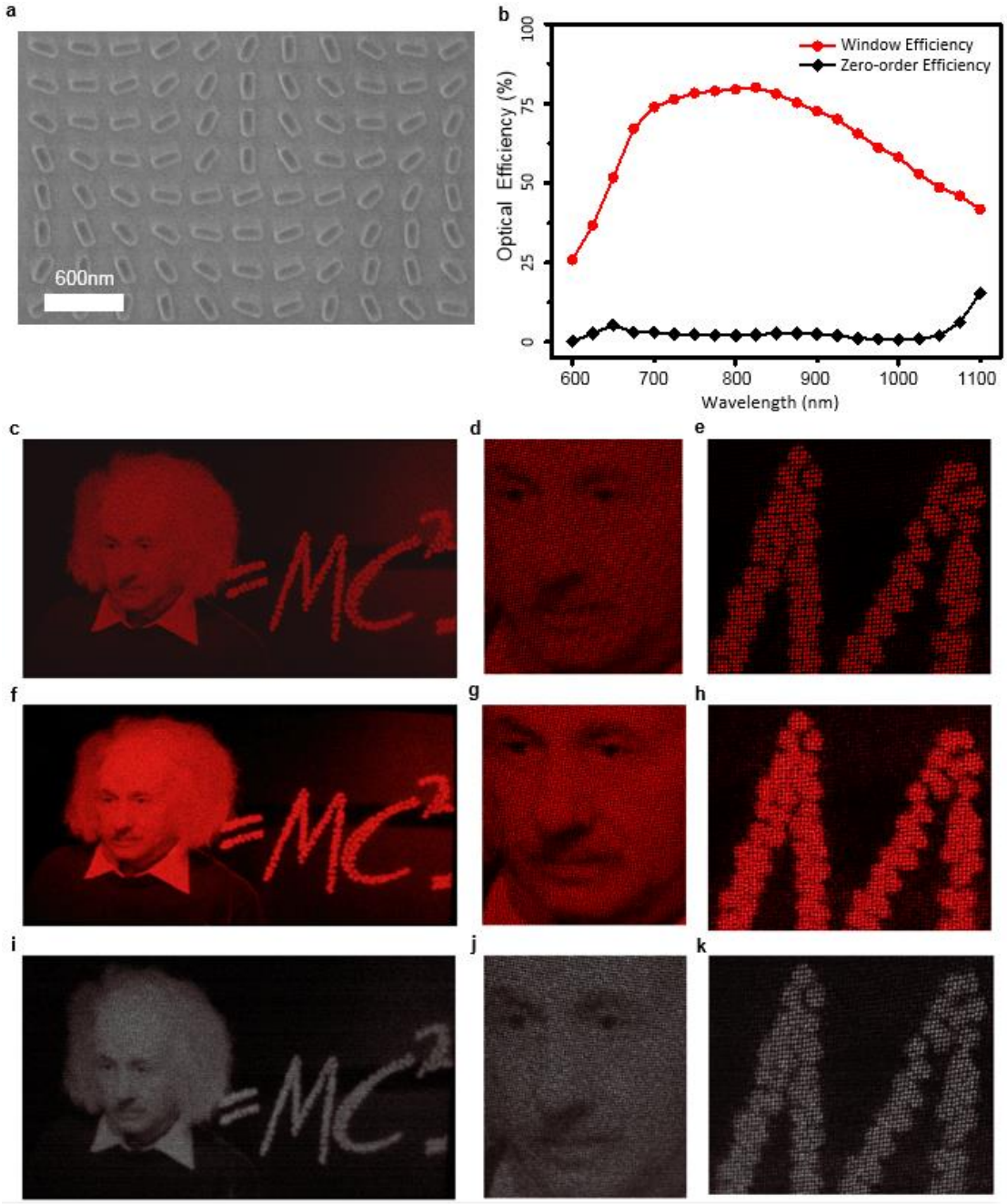

Figure 3 | Experimental results for the holographic image generation. **a**, Scanning electron microscopy image of the fabricated nanorod array (partial view). **b**, Experimentally obtained optical efficiency for both image and 0^{th}-order beam. The measurements show very high optical efficiency above 50% for the image beam over a range of 630-1050 nm. **c, d and e**, Simulated holographic image of Einstein's portrait with enlarged zoom of his face and the character '*M*'. **f, g and h**, Experimentally obtained images that are captured by a visible camera in a far field. The operation wavelength is 632.8 nm. **i, j and k**, Experimentally obtained images that are captured by an infrared camera in the far field, the operation wavelength is 780 nm.

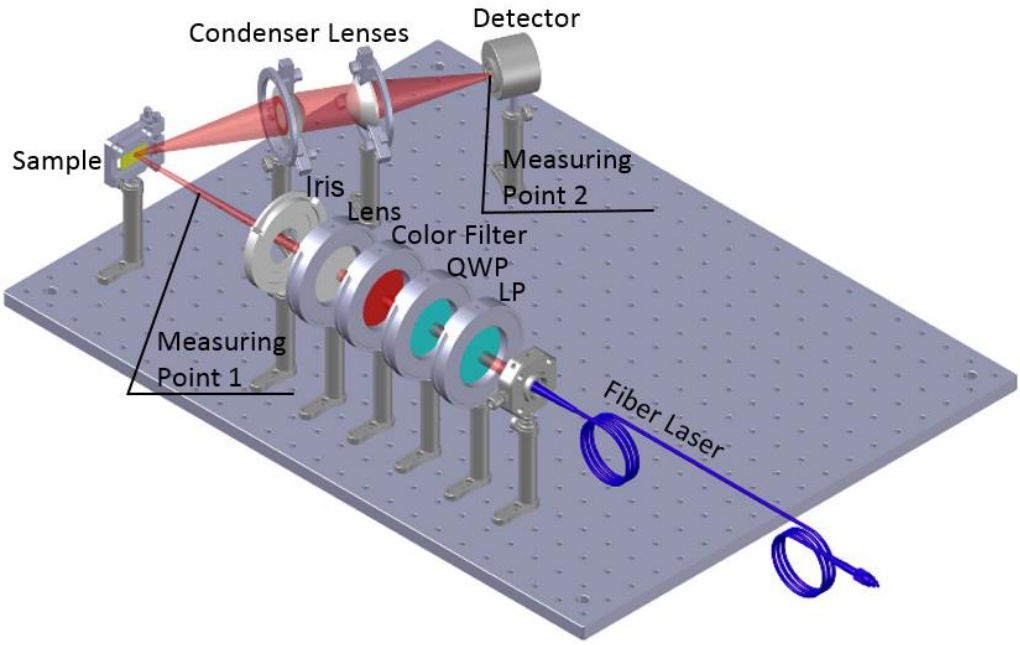

Figure 4 | Illustration of the optical efficiency measurement setup. The incident circularly polarized beam is generated by the linear polarizer (LP) and the quarter waveplate (QWP). The incident circularly polarized beam is focused on the sample and the diffracted light in reflection with opposite circular polarization is collected by two condenser lenses and an optical power detector. For the efficiency measurement, the power was measured at point 1 and 2.